

Solving wave equation problems on D-Wave quantum annealers

Aigerim Bazarkhanova¹, Alejandro J. Castro¹,
Antonio A. Valido^{2*}

¹Department of Mathematics, Nazarbayev University, Kabanbay Batyr
Ave 53, Astana, Kazakhstan.

^{2*}iUNAT, Departamento de Física, Universidad de Las Palmas de Gran
Canaria, 35017 Las Palmas de Gran Canaria, Spain.

*Corresponding author(s). E-mail(s): antonio.valido@ulpgc.es;
Contributing authors: aigerim.bazarkhanova@nu.edu.kz;
alejandro.castilla@nu.edu.kz;

Abstract

We solve the one-dimensional Helmholtz equation in several scenarios using the quantum annealer provided by the D-Wave systems within a pseudospectral scheme, where its solution is encoded into certain set of suitable basis functions. We assess the performance of different strategies of encoding based on algebraic arguments and the adiabatic condition, and benchmark these against the classical heuristic simulating annealing algorithm. In particular, we compute the minimum energy gap, the so-called dynamic range and the mean squared error to assess the numerical stability, consistency and accuracy of the solutions returned by each strategy. Our work stresses out the importance of developing custom embedded techniques ensuring well-conditioned algebraic systems. In particular, we find out that encoding strategies retrieving algebraic systems exhibiting full-rank and small dynamic ranges enhance the performance of the quantum annealer even under polychromatic driving and for intricate initial conditions. We further discuss the prospect of developing hybrid quantum-classical schemes enable to meet suitable algebraic and adiabatic conditions simultaneously.

Keywords: Quantum annealing, D-Wave system, Helmholtz equation, Adiabatic Quantum Computation, Circulant ansatz, Truncated Fourier ansatz

1 Introduction

Wave equation problems play a fundamental role in various fields of physics and engineering, including electromagnetism [1], acoustics, and quantum mechanics [2]. A Fourier analysis is commonly applied by assuming time-harmonic solutions characterized by a certain frequency, which eventually leads to the study of the so-called Helmholtz equation [3]. Numerically solving the latter poses significant challenges depending on the boundary conditions and the geometry of the problem, particularly in high-frequency regimes where the wavelength may be substantially small compared to the characteristic domain size [4]. Traditional computational techniques such as finite difference methods [5, 6], finite element or spectral methods [7, 8] offer effective solutions, but their complexity grows substantially with increasing problem size [9]. This motivates the exploration of alternative approaches, including quantum computing.

Quantum annealing (QA) is a heuristic quantum variational algorithm designed to solve quadratic unconstrained binary optimization (QUBO) problems by encoding their solution in the ground state of a programmed quantum Ising Hamiltonian [10, 11]. This scheme relies on the adiabatic quantum computation paradigm [12], which pursues to evolve a quantum system sufficiently slowly from an initial easy-to-prepare state to a desired final state (that encodes the problem solution). Unlike gate-based quantum computing, which relies on unitary operations and error correction, QA exploits quantum tunneling and superposition to explore multiple solutions simultaneously [13, 14], making it particularly suitable for combinatorial optimization problems [15]. Interestingly, QA has been recently applied to solve partial differential equations by combining finite element, machine learning and iterative methods: these works have shown that it is possible to solve differential equations using quantum annealing [16–18]. However, the extent to which QA provides a superior accuracy and efficiency for a broad class of wave equation problems and scenarios remains an active area of research, with ongoing investigations into its efficiency relative to high-performance classical heuristic algorithms [10], such as the famous simulated annealing (SA) procedure [19].

In the present work we further extend the study of QA combined with spectral methods to solve the Helmholtz equation using the largest commercially available quantum annealers provided by the company D-Wave systems, which has pioneered the development of commercial QA, demonstrating their application in areas such as logistics, machine learning, and materials science [20]. A key challenge of this task lies on encoding the solution of the Helmholtz equation into the D-Wave quantum processing unit (QPU), which imposes constraints on the way the problem variables interact: the Helmholtz equation often leads to densely coupled quantum Ising Hamiltonians with intricate energy landscapes, requiring minor embedding techniques to map logical variables onto the sparse quantum hardware. This embedding process eventually introduces additional computational overhead, potentially impacting the performance of quantum solutions. Here, we explore how this issue could be mitigated by implementing better encoding strategies based on algebraic arguments. In particular, we propose to use the so-called circulant ansatz that retrieves cyclic structure of circulant matrices. Another important question is to which extent the evolving quantum

Ising Hamiltonian satisfies the main adiabatic quantum computation condition characterized in terms of the so-called minimum energy gap [21, 22]. In this line, we also investigate the performance of a more sophisticated ansatz, within a hybrid quantum-classical approach, that maximizes the latter and returns a higher success rate. To evaluate the practical performance of our approach, we benchmark our quantum solver against the SA procedure by using several metrics: the mean squared error that retrieves the accuracy of the obtained solutions, the dynamic range (borrowed from signal processing) in order to evaluate the numerical stability of the QUBO formulation, and the minimum energy gap that permits to assess the consistency with the adiabatic condition. Moreover, as noted in previous studies [23, 24], our results highlight the fundamental role played by the encoding strategies in order to obtain higher success rates and lower mean squared errors.

2 Helmholtz equation in D-Wave systems

In this section we first describe the mathematical framework for the Helmholtz equation and briefly illustrate the standard formulation followed to solve it by the SA technique in classical computers as well as by the QUBO method in the QA provided by D-Wave systems. Afterward, we discuss the main issues behind this procedure and elaborate on the proposed ansatz to sort them out.

2.1 Pseudospectral approximation and simulated annealing

The one-dimensional Helmholtz equation reads

$$\begin{cases} u''(x) + \tau^2 u(x) = F(x), \\ u(0) = \alpha, u'(0) = \beta, \end{cases} \quad (1)$$

where $u(x)$ is a real, continuous, "well-behaved" scalar function (namely, potential) defined in the interval $x \in [0, 2\pi]$, with $\alpha \in \mathbb{R}$ and $\beta \in \mathbb{R}$ representing mixed boundary conditions, and τ is some constant, which is related to the frequency via some appropriate dispersion relation. For instance, it corresponds to the wave number of the harmonic wave propagation of the electric field in a linear, homogeneous, isotropic media [1, 25]. We further consider an external electric current or potential source denoted by certain real function $F(x)$, so our analysis encompasses a broad class of scenarios described by the scalar wave equation from electromagnetics [3]. It is well-known that the complexity of the solutions of the Helmholtz equation significantly depend on the boundary conditions and the geometry of the problem [2, 5].

Beside to be ubiquitous in many areas of physics, mathematics and engineering; we have also addressed the problem (1) since its solution admits a closed form expression that allow to assess our procedure [25], i.e.

$$u(x) = u_h(x) + \frac{1}{\tau^2} \int_0^x \sin(\tau(x-s))F(s)ds,$$

where $u_h(x)$ denotes the solution in the homogeneous case, that is

$$u_h(x) = \alpha \cos(\tau x) + \frac{\beta}{\tau} \sin(\tau x), \quad (2)$$

where it clearly manifests the periodic character of the solutions of the wave equation.

From a mathematical point of view, finding an exact solution of (1) constitutes a rather formidable task in most practical situations, especially for high-frequency problems where the wave number is sufficiently large compared to the domain size of the system [26]. Here we follow a spectral approach which basically consists of representing the solution of (1) as a finite expansion in a set of certain global basis (or testing) functions $\phi_i(x)$, that is the pseudospectral approximation [27]

$$u_N(x) \approx \sum_{i=1}^N w_i \phi_i(x), \quad (3)$$

where $w_i \in \mathbb{R}$ are unknown coefficients, and $\phi_i(x)$ must be defined in $x \in [0, 2\pi]$ and are usually required to be orthonormal with respect to some appropriate weight function for convenient reasons [27]. The choice of these basis functions relies on the features of the specific problem we are dealing with: in particular, the Fourier series is naturally employed in the domain of interest, as expected. For programming purposes, the pseudospectral approximation is applied along with a spatial discretization of the Helmholtz equation, so we can reformulate the original problem into a grid of discrete points x_m with $m = 0, 1, \dots, N - 1$, usually called collocation points, i.e.

$$x_m = \frac{2\pi m}{N}. \quad (4)$$

We have considered the collocation points uniformly spaced along the domain $(0, 2\pi)$ to ensure a regular grid. Notice that this choice is commonly employed to simplify interpolation and differentiation in several numerical methods. As a result, we get a $N + 2$ linear system of equations (notice, the two additional linear equations come from the boundary conditions) with N unknowns, that is w_i , which can be compactly expressed as

$$\mathbf{a}\mathbf{w} = \mathbf{b}, \quad (5)$$

where $\mathbf{w} = (w_1, \dots, w_N)^T$, and \mathbf{a} is a $(N + 2) \times N$ real matrix and \mathbf{b} is a $N + 2$ vector which are fully determined from (1) once (3) is substituted. Hence, by solving Eq. (5) we equivalently obtain an approximated solution of the original differential problem (1) evaluated in the grid.

According to algebraic arguments, there is a direct connection between the rank of a matrix and uniqueness of the solution in optimization problems. In other words, if \mathbf{a} does not have full rank, it leads to degenerate solutions (multiple solutions with the same cost) that may eventually cause the annealer to return ambiguous results. Hence, one could expect that an appropriate choice of the set of basis functions which provides full rank may significantly influence the accuracy of the solution (3).

To guarantee the validity of the proposed solution (3) (or, equivalently (5)), one may further impose that the unknown coefficients w_i minimize the (Euclidean) norm of the error function, i.e. $|u(x) - u_N(x)|$. Additionally, by invoking the least square method, we translate the algebraic problem into a variational problem with the following objective function (also called cost function),

$$\mathcal{C}(u_N) = \sum_{m=0}^{M-1} |u_N''(x_m) + \tau^2 u_N(x_m) - F(x_m)|^2 + |u_N(0) - \alpha|^2 + |u_N'(0) - \beta|^2, \quad (6)$$

where the last two terms ensure that the boundary conditions are fully satisfied. Classically, there exist several numerical variational procedures that retrieve the solution of the optimization problem (6) with significant accuracy. To benchmark the performance of the proposed solution, we employ the SA method, which is integrated with the Monte Carlo technique via the Metropolis algorithm [11]. This method can be understood as the classical counterpart of the D-Wave QPU. This approach relies on the observation that the optimization problem (6) is equivalent to finding the lowest energy state of a certain classical Ising Hamiltonian, i.e.

$$H_{\text{Ising}} = \sum_{i,j} q_{ij} w_i w_j + \sum_i l_i w_i + C_0, \quad (7)$$

where the variables $w_i \in \mathbb{R}$ represent classical spin values, and the matrix \mathbf{q} and the vector \mathbf{l} is determined by, respectively, collecting all quadratic and linear terms in (6), whereas C_0 plays no role for the optimization procedure.

In the following section we shall describe how the above procedure can be also accommodated into a (heuristic) variational quantum algorithm which leads us to the QUBO framework for a generic ansatz (3), and finally recast the approximated solution of the Helmholtz equation (1) into the ground state of a quantum Ising Hamiltonian (experimentally) prepared by the D-Wave platform. In Sec. 3 we perform an extensive comparison of the solutions provided by the SA and this quantum counterpart.

2.2 QUBO and D-Wave system

As anticipated in the introduction, the QUBO model provides a direct mapping of the optimization problem (6) onto the hardware employed in QA, making them a widely adopted framework in quantum computing. This basically consists on mapping the unknown coefficients w_i into qubit variables $\omega_i^l \in \{0, 1\}$ [28],

$$w_i = \sum_{l=0}^{n_{\text{spin}}-1} (-1)^{\alpha(l)} \frac{\omega_i^l}{2^l}, \quad (8)$$

where

$$\alpha(l) = \begin{cases} 1, & l = 0, \\ 0, & l \neq 0, \end{cases}$$

with ω_i^l being spin variables that we need to determine, and n_{spin} is the number of spins per variable, such that the solution is expressed as a finite set of bitstrings $\boldsymbol{\omega} \in \{0, 1\}^r$, with $r = N \times n_{\text{spin}}$. After substituting (8) in the linear system of equations (5), the latter can be rewritten as

$$\mathbf{A}\boldsymbol{\omega} = \mathbf{b} \quad (9)$$

where \mathbf{A} is the block-matrix of size $(N + 2) \times r$

$$\mathbf{A} = \left(-\mathbf{a} \mid 2^{-1}\mathbf{a} \mid 2^{-2}\mathbf{a} \mid \dots \mid 2^{-(n_{\text{spin}}-1)}\mathbf{a} \right). \quad (10)$$

Further doing least squares on (9) we obtain

$$\min_{\boldsymbol{\omega} \in \{0,1\}^r} \boldsymbol{\omega}^T \mathbf{Q}\boldsymbol{\omega} + \mathbf{L}\boldsymbol{\omega} + C'_0, \quad (11)$$

where \mathbf{Q} and \mathbf{L} are referred as QUBO matrices and are fully determined from Eq. (6) once the desired ansatz (3) is substituted (see Sec. 2.2.1 and 2.2.2 for further details), that is

$$\mathbf{Q} = \mathbf{A}^T \mathbf{A}, \quad \mathbf{L} = -2\mathbf{b}^T \mathbf{A}, \quad C'_0 = \mathbf{b}^T \mathbf{b}.$$

Observe that C'_0 can be neglected in the optimization procedure. Here it is important to note that the choice of an appropriate number of spins n_{spin} is crucial for achieving an effective formulation of the problem. A low n_{spin} may be insufficient to accurately represent the problem, whereas a high n_{spin} significantly increases the size of the QUBO matrices, leading to greater computational complexity. Therefore, selecting an optimal n_{spin} is essential to balance problem coverage and computational feasibility.

Provided the QUBO matrices where variables $\omega_i \in \{0, 1\}$, we can reformulate Eq.(11) as an equivalent Ising problem

$$\min_{\tilde{\omega} \in \{-1,1\}^r} \tilde{\omega}^T \tilde{\mathbf{Q}}\tilde{\omega} + \tilde{\mathbf{L}}\tilde{\omega} + \tilde{C}'_0, \quad (12)$$

with variables $\tilde{\omega}_i \in \{-1, 1\}$ using the linear transformation $\tilde{\omega}_i = 2\omega_i - 1$. Now we map the solution of (12) into the ground state of certain quantum Ising Hamiltonian \hat{H}_Q , that is

$$\hat{H}_Q = \sum_{i,j} \tilde{Q}_{ij} \hat{\sigma}_i^{(z)} \hat{\sigma}_j^{(z)} + \sum_i \tilde{L}_i \hat{\sigma}_i^{(z)}, \quad (13)$$

by elevating the spin variables $\tilde{\omega}_i$ into spin operators, i.e.

$$\begin{aligned} \hat{\sigma}_i^{(z)} &= (\otimes_{k=1}^{i-1} \hat{I}) \otimes (\hat{\sigma}^{(z)}) \otimes (\otimes_{k=i+1}^r \hat{I}), \\ \hat{\sigma}_i^{(x)} &= (\otimes_{k=1}^{i-1} \hat{I}) \otimes (\hat{\sigma}^{(x)}) \otimes (\otimes_{k=i+1}^r \hat{I}), \end{aligned}$$

where we have introduced the Pauli matrices acting upon the i th qubit of a system endowed with r qubits, that is

$$\hat{\sigma}^{(z)} = \begin{pmatrix} 1 & 0 \\ 0 & -1 \end{pmatrix} \quad \text{and} \quad \hat{\sigma}^{(x)} = \begin{pmatrix} 0 & 1 \\ 1 & 0 \end{pmatrix},$$

with \hat{I} and \otimes representing the 2×2 identity matrix and the tensorial product operation, respectively. As expected, the size of the quantum Ising Hamiltonian in matricial form is 2^r . Hence, the D-Wave system determines the ground state by performing a quantum annealing procedure characterized by certain time-dependent Ising Hamiltonian [11]

$$\hat{H}_{\text{Ising}}(t) = (1 - t/T)\hat{H}_0 + (t/T)\hat{H}_Q, \quad (14)$$

where

$$\hat{H}_0 = \sum_i \hat{\sigma}_i^{(x)},$$

and T is the maximum time allocated for the evolution to run. The above scheme is based on the adiabatic theorem, which establishes that if the Hamiltonian parameters change sufficiently slow, the system remains close to its ground state, provided that it starts in the ground state of the initial Hamiltonian \hat{H}_0 or, in other words, the D-Wave systems turns into a state very close to the ground state of \hat{H}_Q that can be completely measured, which is equivalent to find the numerical solution of the original problem (6) [10]. This eventually ensures that the desired solution of the optimization problem (11) is achieved. More specifically, the adiabatic theorem states that T must be sufficiently large compared with the energy spectral gap of (14) [12], that is

$$T = O\left(\frac{1}{g_{\min}^2}\right), \quad (15)$$

where minimum energy gap is [29]

$$g_{\min} = \min_{t \in [0, T]} |\lambda_1(t) - \lambda_0(t)| \quad (16)$$

with $\lambda_0(t)$ and $\lambda_1(t)$ be the lowest eigenvalues of $\hat{H}_{\text{Ising}}(t)$. Nonetheless, in practical scenarios, environmental noise, thermal fluctuations, and finite annealing times make the D-Wave system perform a heuristic variational quantum algorithm so that the above adiabatic condition is not completely satisfied. We also pay attention to this point and compute the energy spectral gap for the Hamiltonian (14) in several experiments. In particular, in Sec. 3.2 we further explore the influence of the energy spectral gap on the performance of the QA by considering a generic ansatz built on the adiabatic prescription. Here, it is important to notice that the computation of the spectral gap (16) gets computationally time-consuming for large values of the QUBO matrices due to the size of the quantum Ising Hamiltonian growing exponentially.

From a classical computational perspective, the task of obtaining the global minimum of (6) (which immediately determines the coefficients w_i that exactly solve (5) at the collocation points (4)) becomes rather difficult when the energy landscape of the classical Ising Hamiltonian (7) manifests a large number of local minima [11]. Simultaneously, from the quantum computational perspective, the restricted connectivity of the D-Wave system poses a challenge when mapping the (discretized) Helmholtz problem (5) to the quantum spin system. Since binarization makes matrix \mathbf{A} (9) larger,

it follows that the numerical solution requires long-range couplings in the QUBO matrices that may exceed the native connectivity of D-Wave’s architecture, represented by the Chimera or Pegasus connectivity graphs [30]. To faithfully accommodate a highly sparse QUBO matrix, the D-Wave quantum processor must employ minor embedding, such that logical qubits representing the problem variables are mapped onto multiple physical qubits, effectively increasing connectivity at the cost of introducing additional noise and overhead [10]. In summary, by selecting a basis-function set that maximizes the rank (ensuring a unique, well-conditioned problem) and reduces the sparsity (enhancing embedding efficiency and reducing noise) of the matrix \mathbf{A} , we further contribute to increase the convergence and the accuracy of the heuristic variational quantum annealing process performed by the D-Wave system to solve the Helmholtz equation (1).

Our numerical and experimental results support that the above intuition holds in the classical as well as quantum scenario. Concretely, we have extensively compare the performance of the SA and QA schemes for two choice of the basis functions: one corresponds to the truncated Fourier series that retrieves low-rank and dense \mathbf{A} matrices (see Sec. 2.2.1), and the other one, it is the circulant ansatz which provides full-rank, well-structured, banded matrices \mathbf{A} , reducing embedding complexity (see Sec. 2.2.2).

2.2.1 Truncated Fourier Ansatz

Attending to the periodic properties of the solution of the Helmholtz equation, one may consider the standard basis functions: that is, $\phi_n(x) = \sin(nx)$ or $\phi_n(x) = \cos(nx)$. We then express the function (3) as an expansion in terms of the truncated Fourier series as

$$u_N^{TFA}(x) = \sum_{n=1}^{N/2} (w_n^1 \cos(nx) + w_n^2 \sin(nx)), \quad (17)$$

where w_n^1, w_n^2 are the expansion coefficients - spin variables. Once the ansatz (17) is substituted in the expression of the basis function (3), we obtain a compact matrix form \mathbf{a}^{TFA} , which is a dense matrix where almost all entries are nonzero (see Eq.A.1 in App. A.1). Hence, in the context of QA, it might significantly slow down computations, making them impractical for large-scale quantum computations.

Notice that the truncated Fourier series is widely used in solving partial differential equations [31], especially when the problem exhibits periodicity, as it transforms differential operators into algebraic equations in Fourier space. It is well-known that this spectral method provides high accuracy compared to traditional finite difference or finite element methods [32].

2.2.2 Circulant Ansatz

Now we introduce the circulant ansatz, it reads [33–35],

$$u_N^{CA}(x) = \sum_{n=0}^{N-1} w_n h_n(x), \quad (18)$$

where the auxiliary functions

$$h_n(x) = \frac{1}{N} \sum_{k=-N/2}^{N/2} \frac{1}{c_k} e^{ik(x-x_n)},$$

x_n refers to the collocation points in (4) and

$$c_k = \begin{cases} 1, & |k| < N/2, \\ 2, & |k| = N/2. \end{cases}$$

Interestingly, this choice retrieves a circulant matrix, namely \mathbf{a}^{CA} , see Eq. (A2) in App. A.2. This is a special class of structured matrices where each row is a cyclic shift of the previous one. Indeed, it is already known that the structure of circulant matrices makes them suitable for the application of numerical methods, particularly in solving differential equations, image processing, and fast algorithms [36].

3 Experimental results

In this section we present an extensive comparative analysis of QA performance using the previously introduced ansatz conducted on the D-Wave QA system, with different number N of elements in the approximated solution and the number n_{spin} of spins, to compute approximate solutions of the Helmholtz equation (1) under a range of problem configurations. Specifically, we explore different values of the wave number τ , various combinations of boundary conditions defined by parameters α and β , and several choices for the source term $F(x)$. This diverse experimental setup encompasses a wide spectrum of realistic scenarios, thereby providing a robust testbed for assessing the impact of ansatz structure and encoding strategy on the QA optimization process. Observe that the binary nature of ω ($\omega = \omega^2$) allows us to reformulate the QUBO matrix (11) more compactly by adding the linear terms \mathbf{L} on the diagonal of the quadratic component \mathbf{Q} and obtain

$$\min_{\omega \in \{0,1\}^r} \omega^T \mathbf{Q} \omega + C'_0. \quad (19)$$

We have run the Advantage QPU with the chimera architecture multiple times, that is $n_{\text{run}} = 1000$, with identical conditions for each experiment and assess the

accuracy of the returned solution by means of the metric mean squared error (MSE) i.e.

$$\text{MSE} = \frac{1}{n} \sum_{i=1}^n \left(u(y_i) - u_N(y_i) \right)^2,$$

where n corresponds to the number of evenly spaced points across the interval $(0, 2\pi)$, $u(y_i)$ is the actual value of the exact solution retrieved by Eq. (2) provided the driving force and the initial conditions, and $u_N(x_i)$ is the value obtained from the QA endowed with the TFA (17) or CA (18). Since we are dealing with an heuristic algorithm it is also convenient to evaluate the performance of the QA endowed with a particular ansatz by the so-called success rate (SR), which corresponds to the number of times (out of 1000) D-Wave could return exact solution. Simultaneously, we benchmark QA performance against the classical SA algorithm, implemented using the software suite provided by D-Wave.

For our future analysis we also study the dynamic range (DR) of the QUBO matrix, which can be understood as a measure of the stability of the problem, frequently encountered in imaging or recorded sound. This is defined as follows

$$\text{DR}(\mathcal{Q}) = \log_2 \left(\frac{\hat{D}(\mathcal{Q})}{\check{D}(\mathcal{Q})} \right), \quad (20)$$

where $\hat{D}(\mathcal{Q})$ and $\check{D}(\mathcal{Q})$ denote the absolute value of maximum and minimum entries of \mathcal{Q} , respectively. Notice that we consider nonzero values in the denominator [37].

Finally, we analyze the minimum energy gap associated with the evolving quantum Ising Hamiltonian, as defined in equation (16). Motivated by the fact that the latter play a crucial role in the adiabatic evolution and directly influences the likelihood of the system remaining in its ground state during annealing, we further study the QA performance for an alternative ansatz which completely relies on the maximization of the spectral gap in the last part of this section. Accordingly, we must bear in mind that rank, DR, and g_{min} play the role of indicators to predict the performance of the QA endowed with the aforementioned ansatz, while SR and MSE assess its actual performance.

3.1 Algebraic prescription: Truncated Fourier and Circulant ansatzes

This section presents the results for the aforementioned metrics when we consider the ansatz introduced previously (see Secs. 2.2.1 and 2.2.2) to solve the Helmholtz equation in several scenarios: that involves the inhomogeneous Helmholtz equations with rational and irrational initial conditions, and subject to either monochromatic or polichromatic drivings. As anticipated before, the computation of g_{min} becomes rapidly computationally time-consuming when n_{spin} increases, making unfeasible its evaluation for larger values of N was infeasible.

3.1.1 Homogeneous Helmholtz equation

To get hands-on with the proposed encoding strategies, we begin with the homogeneous Helmholtz equation with trivial initial conditions, that is

$$\begin{cases} u''(x) + u(x) = 0, 0 < x < 2\pi, \\ u(0) = \frac{1}{2}, u'(0) = 0. \end{cases} \quad (21)$$

The exact solution of this problem can be readily obtained from (2), i.e. $u(x) = 1/2 \cos(x)$. From here follows that setting the parameters $N = 2$ and $n_{spin} = 2$ is sufficient to completely embed $u(x)$ in the proposed solution (3) for any of the interested basis functions, so we could expect that both SA and QA (carried on the D-Wave systems) will be able to exactly solve the problem (21). However, in a practical scenario, unless we have some previous information about the latter, the number of basis functions N (in the proposed solution Eq. (3)) or the number of spins n_{spin} (employed in the QUBO) should be eventually updated, either by increasing or decreasing them, following a systematically iterative procedure.

Table 1 The rank, DR and energy minimum gap returned by both ansatz, TFA and CA, are shown for different values of the number of spins, while maintaining fixed the number of basis functions, i.e. $N = 2$. The last two columns show a comparison of the SR achieved by both SA and QA.

n_{spin}	rank(\mathbf{a})		DR(\mathcal{Q})		g_{min}		SR SA (%)		SR QA (%)	
	TFA	CA	TFA	CA	TFA	CA	TFA	CA	TFA	CA
2	2	2	3.321	4.704	19.990×10^{-2}	9.994×10^{-2}	97.1	99.6	99.3	87.1
3	2	2	5.321	6.704	5.294×10^{-2}	2.572×10^{-2}	81.4	97.8	65.8	32.0
4	2	2	7.321	8.704	15.625×10^{-3}	7.814×10^{-3}	52.4	56.1	15.8	6.6
5	2	2	9.321	10.704	3.906×10^{-3}	1.958×10^{-3}	36.8	28.0	3.1	1.2

Since QA as well as SA return the exact solution for the explored parameter set, we employ the indicator SR to assess the performance of both ansatz. Table 1 illustrates the results obtained for the latter together with the rest of the metrics when we change n_{spin} while maintaining fixed the number of basis functions. Overall, we find out that the TFA demonstrates a slightly better performance for both platforms, SA and QA, in agreement with our previous algebraic arguments: TFA retrieves a marginally higher SR and minimum energy gap for most values of n_{spin} . As expected, one may also observe that the SR of the QA scheme substantially diminishes compared to the SA as g_{min} approaches zero with increasing n_{spin} (recall that the quantum Hamiltonian matrix grows as $2^{N \times n_{spin}}$). This result stems from the adiabatic theorem: that is, a longer evolution time to maintain adiabaticity in QA is required when g_{min} decreases according to (15), which becomes experimentally harder due to the thermal fluctuations, bias leakage and other technical issues.

3.1.2 Inhomogeneous Helmholtz equation with monochromatic driving I

Now we consider the influence of a monochromatic driving in the SA and QA performance, i.e.

$$\begin{cases} u''(x) + u(x) = \frac{3}{2} \cos 2x, 0 < x < 2\pi, \\ u(0) = 0, u'(0) = 0. \end{cases} \quad (22)$$

The exact solution is $u(x) = 1/2(\cos x - \cos 2x)$, so we shall take at least $N \geq 4$ and $n_{spin} \geq 2$. Here we are interested in analyzing how the pseudospectral approximation, endowed with TFA and CA, works under the presence of a driving force. We begin studying several figures of merit: rank, DR, g_{min} , SR for SA and QA as a function of the spin number with fixed $N = 4$, the results are shown in Table 2. A quick glance reveals that an increasing n_{spin} makes DR become larger, while the minimum gap diminishes toward zero, which eventually turns into a decreasing SR for both SA and QA. This is expected since the Hamiltonian size grows.

Table 2 The rank, DR and energy minimum gap returned by both ansatz, TFA and CA, are shown for different values of the number of spins, while maintaining fixed the number of basis functions, i.e. $N = 4$. The last two columns show a comparison of the SR achieved by both SA and QA.

n_{spin}	rank(\mathbf{a})		DR(\mathcal{Q})		g_{min}		SR SA (%)		SR QA (%)	
	TFA	CA	TFA	CA	TFA	CA	TFA	CA	TFA	CA
2	3	4	54.619	8.159	1.662×10^{-3}	1.535×10^{-1}	41.1	79.11	11.2	23
3	3	4	56.619	10.189	2.787×10^{-3}	3.882×10^{-2}	18.8	33	1.3	2.5

From Table 2 one may further observe that the TFA yields a rank-deficient matrix, while the CA produces a full-rank matrix for $n_{spin} = 2, 3$. According to the discussion of Sec. 2, this indicates that the former method may lead to a large number of false positives in comparison with the second method. A comparison of the two methods shows that DR is consistently larger for the TFA. Notably, the SA and QA results are consistently better for the CA (i.e. it is almost double compared to TFA), indicating its greater robustness and reliability under increasing model complexity.

Table 3 The rank, DR and MSE for SA and QA returned by both ansatz, TFA and CA, are shown for different values of the number of basis functions, while maintaining fixed the number of spins, i.e. $n_{spin} = 2$.

N	rank(\mathbf{a})		DR(\mathcal{Q})		MSE (SA)		MSE (QA)	
	TFA	CA	TFA	CA	TFA	CA	TFA	CA
4	3	4	54.619	8.189	0	0	0	0
8	7	8	65.796	56.579	0	0.011	0	0
10	9	10	65.077	57.803	0	0.026	0.124	0.044
18	17	18	69.398	59.189	0	0.065	0.5	0.241

Now we fix $n_{\text{spin}} = 2$ and investigate how increasing N influences MSE, as well as the rank and the DR. The results are shown in Table 3. Based on the rank analysis, the TFA method exhibits rank deficiency, whereas the second method, CA, consistently yields a full-rank matrix for all values of N . Although the DR is relatively large for both ansatzes, it is notably smaller for the CA method. Furthermore, the MSE is also lower for the QA endowed with the CA, while for SA equipped with the TFA performs better. These results suggest that maintaining full rank and achieving a relatively smaller DR value contribute to improved model accuracy in QA, as reflected in the decreasing of the MSE.

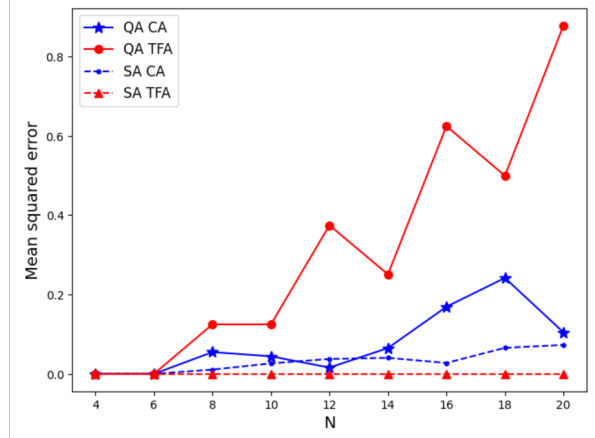


Figure 1 (color online) MSE, retrieved by SA and QA in the scenario (22), as a function of the number N of spin functions for a fixed value of the number of spins, i.e. $n_{\text{spin}} = 2$.

Figure 1 illustrates the MSE for SA and QA returned by both ansatz, TFA and CA, as a function of N . Since the size of the QUBO matrix is growing, we could only conduct $N = 4, \dots, 20$. Across all experiments, the lowest MSE appears for the SA procedure when we use TFA. However, it is evident that in the quantum setting, CA (blue solid line) approximates better than TFA (red solid line). Overall, increasing N hinders the effort to find the ground state. Other practical issues would also affect the performance: such as round-off errors during the QUBO/Ising preparation and the hardware precision for the Ising coefficients.

Finally, Fig. 2 shows the approximate solution u_N , returned by QA endowed with both ansatzes, in comparison with the exact solution. More concretely, the upper panel illustrates this for increasing values of the number of spins, $n_{\text{spin}} = 2, 8, 10$ (from left to right), whereas the lower panel depicts this for increasing values of the number of basis functions, $N = 4, 10, 18$ (from left to right). Clearly, one may observe that across all three cases, the CA consistently demonstrates better performance than the TFA.

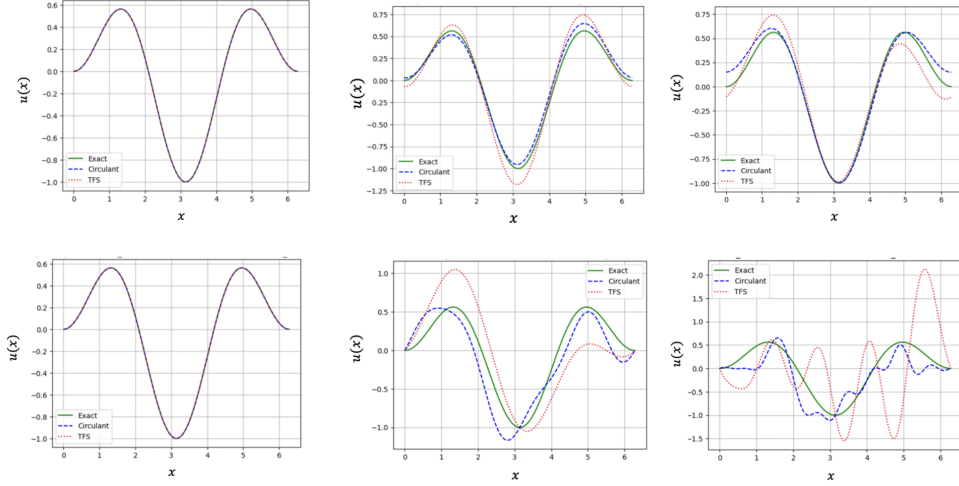


Figure 2 (Upper row) Exact and approximated solution returned by QA endowed with TFA and CA for increasing number of spins, $n_{\text{spin}} = 2, 8, 10$ from left to right, and fixed $N = 4$. (Lower row) Similarly, exact and approximated solution returned by QA endowed with TFA and CA for increasing number of basis functions, $N = 4, 10, 18$ from left to right, and fixed $n_{\text{spin}} = 2$.

3.1.3 Inhomogeneous Helmholtz equation with monochromatic driving II

In this section, we further investigate the performance of QA when we combine a higher-frequency monochromatic driving with a larger wave number, i.e. $\tau = 2$. Concretely, we study the problem

$$\begin{cases} u''(x) + 4u(x) = -6 \cos 4x, 0 < x < 2\pi, \\ u(0) = \frac{1}{2}, u'(0) = 1, \end{cases} \quad (23)$$

whose exact solution is $u(x) = 1/2(\cos 4x + \sin 2x)$. From expression (23) then follows that the ground state energy would be precisely achieved when $N = 8$, and we anticipate that our results confirm this observation. As pointed out, selecting the correct parameter set is important for attaining the lowest energy state: in particular, for this experiment, $n_{\text{spin}} = 2$ proves to be sufficient.

Similarly as before, we fix the number of spins and explore the effects of increasing N upon the interesting figure of merits, the results are shown in Table 4. The rank analysis reveals that the TFA method suffers from rank deficiency once again, whereas the CA method consistently maintains a full-rank matrix. While the DR is relatively high for both ansatz, it is lower in the case of CA. Additionally, the CA method yields lower MSE values. These findings are consistent with previous results and indicate that preserving a full rank matrix \mathbf{a} and minimizing the DR are beneficial for enhancing model accuracy, as evidenced by the reduced MSE for QA. Interestingly, by paying attention to the MSE(QA) column in Table 4 for both ansatz, one may observe that

Table 4 The rank, DR and MSE for SA and QA returned by both ansatz, TFA and CA, are shown for different values of the number of basis functions, while maintaining fixed the number of spins, i.e. $n_{\text{spin}} = 2$.

N	rank(\mathbf{a})		DR(\mathcal{Q})		MSE (SA)		MSE (QA)	
	TFA	CA	TFA	CA	TFA	CA	TFA	CA
4	4	4	56.619	58.064	0.495	1.251	0.125	1.054
8	7	8	66.655	59.184	0.247	$\mathbf{0}$	0.124	$\mathbf{0}$
10	9	10	64.107	58.201	0.247	0.008	0.125	0.041
18	17	18	69.288	59.112	0.247	0.027	0.501	0.145

the QA endowed with the CA retrieves lower values of MSE compared to the TFA, supporting our observation that well-conditioning algebraic conditions could help to mitigate noise and control error effects.

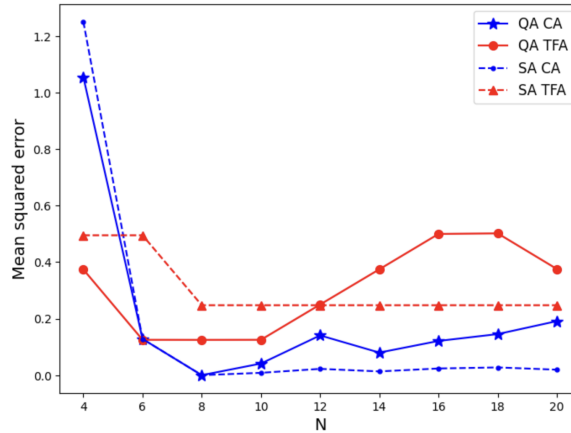


Figure 3 (color online) MSE, retrieved by SA and QA in the scenario (23), as a function of the number N of spin functions for a fixed value of the number of spins, i.e. $n_{\text{spin}} = 2$.

Interestingly, from Fig. 3, one may observe that the CA ansatz successfully returns the solution for $N = 8$ and $n_{\text{spin}} = 2$, while the TFA ansatz fails to achieve comparable performance for any value of the number of basis functions. These results emphasize that the CA ansatz is better suited for involved initial conditions in agreement with the discussion of Sec. 2.2. One may also observe from Fig. 4 that the CA method outperforms the TFA method for several values of the number of spins as well (see the left panel in the upper and lower rows). We further observe that an increasing number N makes the QA (combined with either the CA or the TFA) to fail as the MSE increases, while the MSE returned by the SA (endowed with either the CA or the TFA) barely changes. This could be understood by recalling that the embedding task of mapping the problem (23) to quantum hardware may increase crosstalk and control errors as N or n_{spin} grow. This eventually makes the adiabatic conditions harder to be satisfied, which eventually degrades the performance of the QA.

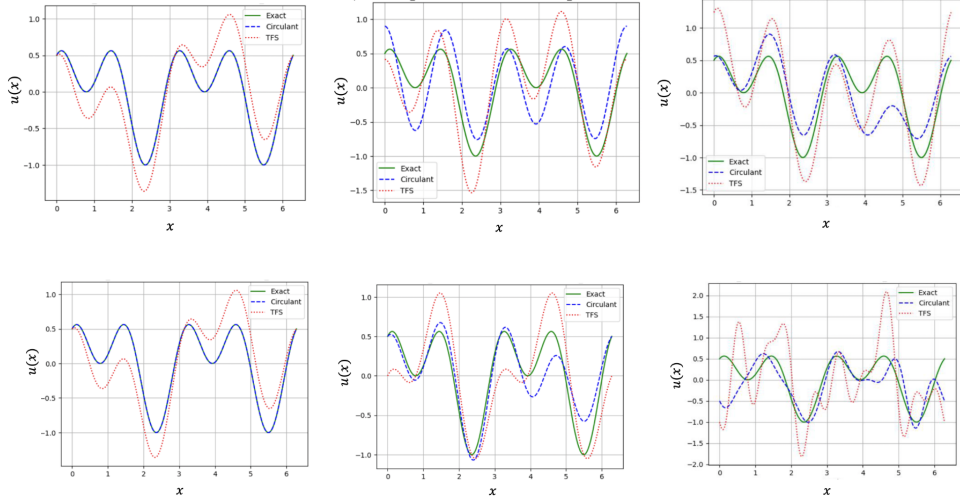


Figure 4 (Upper row) Exact and approximated solution returned by QA endowed with TFA and CA for a fixed number of basis functions (i.e. $N = 4$) and an increasing number of spins: $n_{\text{spin}} = 2, 8, 10$ from left to right, respectively. (Lower row) Similarly, exact and approximated solution returned by QA endowed with TFA and CA for a fixed number of spins (i.e. $n_{\text{spin}} = 2$) and an increasing number of basis functions: $N = 4, 10, 18$ from left to right, respectively.

3.1.4 Inhomogeneous Helmholtz equation with polychromatic driving

In this section we pay attention to practical involved situations where the driving is polychromatic, such as

$$\begin{cases} u''(x) + u(x) = 2 \cos 3x - \frac{15}{4} \cos 4x - \frac{3}{4} \sin 2x + 2 \sin 3x, 0 < x < 2\pi, \\ u(0) = -\frac{1}{4}, u'(0) = 0. \end{cases} \quad (24)$$

whose exact solution is

$$u(x) = \frac{1}{4}(-\cos(x) - \cos(3x) + \cos(4x) + \sin(x) + \sin(2x) - \sin(3x)).$$

From this expression follows that the solution becomes rather involved for the studied polychromatic driving. Overall, the results obtained here are consistent with the discussion of Secs. 2.2 and 3.1.3: the solution retrieved by QA, endowed with the CA, exhibits higher accuracy according to the fact that a full rank matrix \mathbf{a} and a lower DR may contribute to substantially diminish the MSE even in polychromatic scenarios.

Here, we fix the number of spins to $n_{\text{spin}} = 3$ since representing the initial condition $\alpha = 1/4$ in binary form requires at least three spins. Similarly as before, we study how a growing number N of basis functions influences the performance of rank, DR and MSE in both ansatz. These results are illustrated in Table 5. As expected, the CA produce

a full rank matrix \mathbf{a} unlike the TFA, as well as the former returns comparatively lower values of DR as occurs in Sec. 3.1.3 (though this could be relatively high). Notice that the CA retrieves once again the lowest MSE value.

Table 5 The rank, DR and MSE for SA and QA returned by both ansatz, TFA and CA, are shown for different values of the number of basis functions, while maintaining fixed the number of spins, i.e. $n_{\text{spin}} = 3$.

N	$\text{rank}(\mathbf{a})$		DR(Q)		MSE(SA)		MSE(QA)	
	TFA	CA	TFA	CA	TFA	CA	TFA	CA
4	3	4	58.781	9.303	0.154	1.280	0.124	0.919
8	7	8	68.211	60.261	0.185	0.015	0.125	0.054
10	9	10	67.076	60.492	0.185	0.006	0.187	0.145
18	17	18	71.398	61.270	0.185	0.035	0.688	0.236

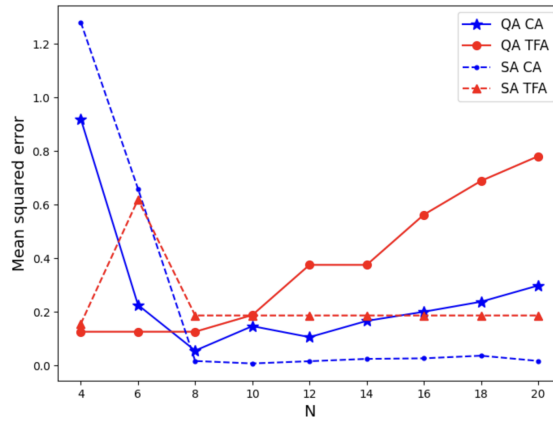


Figure 5 (color online) MSE, retrieved by SA and QA in the scenario (24), as a function of the number N of spin functions for a fixed value of the number of spins, i.e. $n_{\text{spin}} = 3$.

Figure 5 further illustrate the MSE returned by both ansatz in the SA and the QA for a growing number N of basis functions and a fixed spin number, i.e. $n_{\text{spin}} = 3$. From a preliminary Fourier analysis based on Eq. (2.1) is expected that both annealing procedures retrieve the ground state for $N = 8$. This is observed in Fig. 5 where MSE vanishes exactly for $N = 8$. Interestingly, we also observe that SA, endowed with either the CA or the TFA, converges as N increases in contrast to QA.

3.1.5 Homogeneous Helmholtz equation with irrational initial conditions

The propose of this experiment is to asses the accuracy of the SA and the QA when the initial condition α cannot be exactly represented in binary form unless we take an

infinite large number of spins. Concretely, we now study the following problem

$$\begin{cases} u''(x) + u(x) = 0, 0 < x < 2\pi, \\ u(0) = \frac{\sqrt{2}}{2}, u'(0) = 0, \end{cases} \quad (25)$$

whose exact solution is $u(x) = \frac{\sqrt{2}}{2} \cos(x)$.

Table 6 The rank, DR and MSE for SA and QA returned by both ansatz, TFA and CA, are shown for different values of the number of spins, while maintaining fixed the number of basis function, i.e. $N = 2$.

n_{spin}	$\text{rank}(\mathbf{a})$		$\text{DR}(\mathcal{Q})$		g_{min}		$\text{MSE}(\text{SA})$		$\text{MSE}(\text{QA})$	
	TFA	CA	TFA	CA	TFA	CA	TFA	CA	TFA	CA
2	2	2	6.086	5.479	1.999×10^{-1}	1.029×10^{-1}	0.021	0.021	0.022	0.022
3	2	2	6.149	8.546	4.105×10^{-2}	2.414×10^{-2}	0.001	0.001	0.001	0.001
4	2	2	7.543	8.873	4.902×10^{-3}	4.916×10^{-3}	0.001	0.001	0.001	0.001
5	2	2	9.543	10.873	1.509×10^{-3}	1.953×10^{-3}	0.001	0.001	0.001	0.001

Table 6 shows the results for the rank, the DR and the g_{min} returned by both the CA and the TFA, as well as the MSE obtained from the methods QA and SA endowed with both ansatz. Here, \mathbf{a} becomes a full rank matrix, and the DR increases as the number of spins increases as expected. On the other hand, the minimum energy gap approaches zero as the Hamiltonian size grows, which leads to a corresponding decreasing of SR for both methods (the SA and the QA). This behavior is consistent with the adiabatic theorem, which states that smaller energy gaps require longer evolution times to maintain the adiabaticity prescription (15).

3.2 Adiabatic prescription: adiabatic ansatz

Previously, we have observed that ansatz endowed with higher minimum energy gaps retrieves higher success rates. This observation motivates us to further explore the influence of the energy spectral gap on the choice of the basis function in Eq. (3). Concretely, we now build a generic ansatz by appealing to the adiabatic prescription rather than the previous algebraic arguments: we just require it maximizes the minimum energy spectral gap (16). This alternative ansatz can be expressed as follows

$$u_N = \sum_{n=0}^{N-1} w_n G_n(x), \quad (26)$$

where $\{G_0(x), G_1(x), \dots, G_{N-1}(x)\}$ is a new set of basis functions, i.e.

$$G_n(x) = \sum_{k=-N/2}^{N/2} g_{n,k} e^{ikx},$$

where $g_{n,k}$ are complex coefficients to be determined. Notice that Eq. (26) contains the previously studied ansatz as particular instances, where the coefficients $g_{n,k}$ were picked up to retrieve the Fourier series or to satisfy algebraic prescriptions as occurs in the case of the circulant ansatz. In contrast to these, we now impose that the coefficients $g_{n,k}$ maximize the energy spectral gap (16), which can be computed by numerically diagonalizing the quantum Ising Hamiltonian retrieved by (26) following the procedure described in Sec. 2.2. In particular, we have performed this computation by exploiting Python numerical libraries. The difficulty of diagonalizing the quantum Ising Hamiltonian (14) (recall its size is 2^r) makes the optimization procedure a formidable computational task, so we shall focus the attention on the first experiment illustrated in Sec. 3.1.1 for fixed values $N = 4$ and $n_{\text{spin}} = 2$.

Now using (26) we compute the ansatz that simultaneously minimizes the energy gap (16) and provides an approximate solution to the problem (21). This shall be referred to as adiabatic ansatz (AA). Table 7 show the results retrieved by both methods, QA and SA, when we employ the latter, as well as the previously studied ansatz. Interestingly, one may observe that by increasing g_{\min} as well as ensuring a full rank matrix \mathbf{a} , we are able to achieve significantly higher values of the SR with the QA method: concretely, this represents an improvement around 54% compared to the TFA and 39% compared to the CA. This contrasts with the SA method, where the AA scheme returns a slightly lower SR compared to the CA. The latter could be understood by paying attention to the DR: this takes a value twice as large for the AA compared to the CA. These results are consistent with our previous observation: higher-rank matrices and narrower dynamic ranges enhance the performance of both annealing approaches. The present experiment further suggests that we could develop hybrid encoding schemes that simultaneously provide well-conditioned and stable systems of equations (5) as well as minimize the energy gap. The latter condition guarantees that our setup could eventually meet the experimental restrictions imposed but the adiabatic procedure, whereas the former prescription enhance the problem’s tractability by shaping an energy landscape that avoids degenerate regions and numerical instability.

Table 7 The rank, DR and g_{\min} returned by TFA, CA and AA are shown for $N = 4$, $n_{\text{spin}} = 2$. The last two columns show a comparison of the SR achieved by both SA and QA.

	$\text{rank}(\mathbf{a})$	$\text{DR}(\mathcal{Q})$	g_{\min}	SR SA (%)	SR QA (%)
TFA	3	54.923	4.338×10^{-4}	44.3	8.2
CA	4	7.169	1.229×10^{-1}	65.9	11
AA	4	16.19	1.332×10^{-1}	65.3	18

4 Outlook and conclusion

In this work, we extended the application of QA combined with spectral methods to solve the one-dimensional Helmholtz equation on state-of-the-art quantum hardware provided by D-Wave systems. Our investigation mainly focused on evaluating

the performance of two distinct ansatzes, the TFA and the CA, across different initial conditions and several experimental settings, including the number of spectral components N and binary spins n_{spins} . Our study offers a comprehensive understanding of the strengths and limitations of these encoding strategies for solving the Helmholtz equation, as well as validate the reliability of performing QA under the current hardware constraints.

Our results consistently demonstrated that the CA, which yields full rank matrices across various settings, manifests better overall performance, including lower mean squared errors and higher success rates. In contrast, the TFA frequently led to rank-deficient matrices, which introduced ambiguity in solutions and limited its robustness in practical scenarios. The observed trends in the energy spectral gap, as predicted by the adiabatic theorem, aligns with previous observations, emphasizing the importance of suitable algebraic prescriptions on ansatz design in quantum variational heuristics. In particular, a major contribution of our study lies in identifying the key role played by the rank of the matrix properties of the encoded QUBO problem in influencing the numerical behavior of the QA.

The comparison between quantum and simulated annealing reveals similar qualitative behaviors. In particular, our findings suggest that basis selection and matrix conditioning could mitigate the downfall noise effects and control errors when encoding continuous physical problems into quantum-optimized binary formulations. Collectively, these prescriptions influence the smoothness of the energy landscapes, and thus, they could reduce the likelihood of noisy transitions between near-degenerate solutions, contributing eventually to enhance the robustness of the optimization process under thermal noise.

Although no industrial application has mathematically yet demonstrated a clear superiority of QA over classical methods, our study contributes to understanding how developing custom embedding techniques, that return full-rank matrices with narrow dynamic range while preserving D-Wave’s architectural constraints, could enhance the performance of QA to solve wave equations. As quantum hardware continues to mature, we hope this lies the groundwork for future advancements in quantum solvers for wave equations.

Supplementary information. For supplementary information, the corresponding codes for experiments are provided in the attached files.

Acknowledgements. This work is supported by the Ministry of Education and Science of the Republic of Kazakhstan (Grant No AP19676408).

Appendix A QUBO Derivation

In this appendix, we start illustrating the derivation of the QUBO problem (11) for a general ansatz (3) and in subsections A.1 and A.2 we do it for the TFA and CA ansatzes.

From the Helmholtz equation (1) using (3) and discretization over the N collocation points (4) we get

$$\begin{cases} \sum_{i=1}^N w_i \phi_i''(x_m) + \tau^2 \sum_{i=1}^N w_i \phi_i(x_m) = F(x_m), & m = 0, 1, \dots, N-1 \\ \sum_{i=1}^N w_i \phi_i(0) = \alpha \\ \sum_{i=1}^N w_i \phi_i'(0) = \beta. \end{cases}$$

As a result, we get $N + 2$ linear equations with unknowns $\mathbf{w} = (w_1, w_2, \dots, w_N) \in \mathbb{R}^N$, which can be compactly expressed in matrix form (5). Using the binary encoding (8), we can obtain the system of equations (9) for unknowns

$$\boldsymbol{\omega} = (\omega_1^0, \dots, \omega_N^0, \dots, \omega_1^{n_{spin}-1}, \dots, \omega_N^{n_{spin}-1}) \in \{0, 1\}^r.$$

To reformulate our problem as QUBO we use the least squares method and get (11).

Next we focus on obtaining the matrix \mathbf{a} for each particular case.

A.1 Linear System of Equations for TFA

To obtain a compact matrix form for TFA we refer to the ansatz (17) introduced in Section 3.1.

Following the method described in the preceding section we obtain

$$\mathbf{a}^{TFA} \mathbf{w} = \mathbf{b}$$

where

$$\mathbf{w} = (w_1^1, w_2^1, \dots, w_{N/2}^1, \dots, w_1^2, w_2^2, \dots, w_{N/2}^2) \in \mathbb{R}^N$$

and the coefficient matrix is

$$\mathbf{a}^{TFA} = \begin{pmatrix} c_{0,1} & \cdots & c_{0,N/2} & s_{0,1} & \cdots & s_{0,N/2} \\ \vdots & \ddots & \vdots & \vdots & \ddots & \vdots \\ c_{(N-1),1} & \cdots & c_{(N-1),N/2} & s_{(N-1),1} & \cdots & s_{(N-1),N/2} \\ 1 & \cdots & 1 & 0 & \cdots & 0 \\ 0 & \cdots & 0 & 1 & \cdots & N/2 \end{pmatrix} \quad (\text{A1})$$

for $c_{m,n} = (\tau^2 - n^2) \cos(nx_m)$ and $s_{m,n} = (\tau^2 - n^2) \sin(nx_m)$.

A.2 Linear System of Equations for CA

We proceed with the formulation of the circulant ansatz (18) and obtain compact matrix form as

$$\mathbf{a}^{CA} \mathbf{w} = \mathbf{b}$$

with

$$\mathbf{a}^{CA} = \begin{pmatrix} d_0 & d_\ell & \cdots & d_{(N-2)\ell} & d_{(N-1)\ell} \\ d_{-\ell} & d_0 & d_\ell & \cdots & d_{(N-2)\ell} \\ \vdots & d_{-\ell} & d_0 & \ddots & \vdots \\ d_{-(N-2)\ell} & \vdots & \ddots & \ddots & d_\ell \\ d_{-(N-1)\ell} & d_{-(N-2)\ell} & \cdots & d_{-\ell} & d_0 \\ \hline e_0 & e_\ell & \cdots & e_{(N-2)\ell} & e_{(N-1)\ell} \\ f_0 & f_\ell & \cdots & f_{(N-2)\ell} & f_{(N-1)\ell} \end{pmatrix}$$

and

$$d_{n\ell} = \sum_{k=-N/2}^{N/2} \frac{(\tau^2 - k^2)}{Nc_k} e^{-ikn\ell}, \quad e_{n\ell} = \sum_{k=-N/2}^{N/2} \frac{1}{Nc_k} e^{-ikn\ell}, \quad f_{n\ell} = \sum_{k=-N/2}^{N/2} \frac{ik}{Nc_k} e^{-ikn\ell}$$

for $n\ell = x_n - x_0 = \frac{2\pi n}{N}$. In addition, by the periodicity

$$e^{-ik(N-j)\ell} = e^{-ikN\ell} e^{-ik(-j)\ell} = e^{-ikN\frac{2\pi}{N}} e^{-ik(-j)\ell} = e^{-ik(-j)\ell}$$

we can express

$$\mathbf{a}^{CA} = \begin{pmatrix} d_0 & d_\ell & \cdots & d_{-2\ell} & d_{-\ell} \\ d_{-\ell} & d_0 & d_\ell & \cdots & d_{-2\ell} \\ \vdots & d_{-\ell} & d_0 & \ddots & \vdots \\ d_{2\ell} & \vdots & \ddots & \ddots & d_\ell \\ d_\ell & d_{2\ell} & \cdots & d_{-\ell} & d_0 \\ \hline e_0 & e_\ell & \cdots & e_{(N-2)\ell} & e_{(N-1)\ell} \\ f_0 & f_\ell & \cdots & f_{(N-2)\ell} & f_{(N-1)\ell} \end{pmatrix}. \quad (\text{A2})$$

Observe that the first block of the matrix provides a circulant structure which is a cyclic shift of the previous one.

References

- [1] Van Bladel, J.: *Electromagnetic Fields*. John Wiley and Sons, Inc., Hoboken, New Jersey, Hoboken, New Jersey (2007)
- [2] Arfken, G.B., Weber, H.J.: *Mathematical Methods for Physicists*. Elsevier, Burlington, MA, 93 (2005)
- [3] Chew, W.C.: *Waves and Fields in Inhomogeneous Media*. IEEE Press, New York (1995)
- [4] Ihlenburg, F., Babuska, I.: Finite element solution of the helmholtz equation with high wave number part iil: The hp version of the fem. *SIAM J. Numer. Anal.* **34**(1), 315–358 (1997) [https://doi.org/10.1016/0898-1221\(95\)00144-N](https://doi.org/10.1016/0898-1221(95)00144-N)

- [5] Cohen, G.C.: Higher Order Numerical Methods for Transient Wave Equations. Springer, New York (2002)
- [6] García-Ripoll, J.J.: Quantum-inspired algorithms for multivariate analysis: from interpolation to partial differential equations. *Quantum* **5**, 431 (2021) <https://doi.org/10.22331/q-2021-04-15-431>
- [7] Gumerov, N.A., Duraiswami, R.: Recursions for the computation of multipole translation and rotation coefficients for the 3-d Helmholtz equation. *SIAM J. Sci. Comput.* **25**(4), 1344–1381 (2003) <https://doi.org/10.1137/S1064827501399705>
- [8] Wright, L., Mc Keever, C., First, J.T., Johnston, R., Tillay, J., Chaney, S., Rosenkranz, M., Lubasch, M.: Noisy intermediate-scale quantum simulation of the one-dimensional wave equation. *Phys. Rev. Res.* **6**, 043169 (2024) <https://doi.org/10.1103/PhysRevResearch.6.043169>
- [9] Klaseboer, E., Sun, Q.: Helmholtz equation and non-singular boundary elements applied to multi-disciplinary physical problems. *Commun. Theor. Phys.* **74**(8), 085003 (2022) <https://doi.org/10.1088/1572-9494/ac794a>
- [10] Yarkoni, S., Raponi, E., Bäck, T., Schmitt, S.: Quantum annealing for industry applications: introduction and review. *Rep. Prog. Phys.* **85**(10) (2022) <https://doi.org/10.1088/1361-6633/ac8c54>
- [11] Hauke, P., Katzgraber, H.G., Lechner, W., Nishimori, H., Oliver, W.D.: Perspectives of quantum annealing: Methods and implementations. *Rep. Prog. Phys.* **83**(5), 054401 (2020) <https://doi.org/10.1088/1361-6633/ab85b8>
- [12] Tameem, A., Lidar, D.A.: Adiabatic quantum computation. *Rev. Mod. Phys.* **90**, 015002 <https://doi.org/10.1103/RevModPhys.90.015002>
- [13] Pelofske, E., Hahn, G., Djidjev, H.N.: Solving larger maximum clique problems using parallel quantum annealing. *Quantum Inf.Process.* **22** (2023) <https://doi.org/10.1007/s11128-023-03962-x>
- [14] Rajak, A., Suzuki, S., Dutta, A., Chakrabarti, B.K.: Quantum annealing: An overview. *Phil. Trans. R. Soc. A* **381**(2241), 20210417 (2023) <https://doi.org/10.1098/rsta.2021.0417>
- [15] Willsch, D., Willsch, M., Gonzalez Calaza, C.D., Jin, F., De Raedt, H., Svensson, M., Michielsen, K.: Benchmarking advantage and d-wave 2000q quantum annealers with exact cover problems. *Quantum Inf.Process.* **21**(4), 1–22 (2022) <https://doi.org/10.1007/s11128-022-03476-y>
- [16] Conley, R., Choi, D., Medwig, G., Mroczko, E., Wan, D., Castillo, P., Yu, K.: Quantum optimization algorithm for solving elliptic boundary value problems on d-wave quantum annealing device. In: *Quantum Computing, Communication, and*

Simulation III, vol. 12446, p. 124460 (2023). <https://doi.org/10.1117/12.2649076>

- [17] Góes, C.B.D., Maciel, T.O., Pollachini, G.G., Salazar, J.P.L., Cuenca, R.G., Duzzioni, E.I.: Qboost for regression problems: solving partial differential equations. *Quantum Inf.Process.* **22**(2) (2023) <https://doi.org/10.1007/s11128-023-03871-z>
- [18] Srivastava, S., Sundararaghavan, V.: Box algorithm for the solution of differential equations on a quantum annealer. *Phys. Rev. A* **99**, 052355 (2019) <https://doi.org/10.1103/PhysRevA.99.052355>
- [19] Bertsimas, D., Tsitsiklis, J.: Simulated annealing. *Stat. Sci* **8**(1), 10–15 (1993) <https://doi.org/10.1214/ss/1177011077>
- [20] King, A.D., Nocera, A., Rams, M.M., Dziarmaga, J., Wiersema, R., Bernoudy, W., Raymond, J., Kaushal, N., Heinsdorf, N., Harris, R., *et al.*: Beyond-classical computation in quantum simulation. *Science* **388**(6743), 199–204 (2025) <https://doi.org/10.1126/science.ado6285>
- [21] Borle, A., Lomonaco, S.J.: How viable is quantum annealing for solving linear algebra problems? arXiv preprint arXiv:2206.10576 (2022)
- [22] Isermann, S.: On the optimal schedule of adiabatic quantum computing. *Quantum Inf.Process.* **20**(9) (2021) <https://doi.org/10.1007/s11128-021-03227-5>
- [23] Schuld, M., Sweke, R., Meyer, J.J.: Effect of data encoding on the expressive power of variational quantum-machine-learning models. *Phys. Rev. A* **103**(3), 032430 (2021) <https://doi.org/10.1103/PhysRevA.103.032430>
- [24] Hunout, J., Laizet, S., Iannucci, L.: Variational quantum algorithm based on lagrange polynomial encoding to solve differential equations. *Phys. Rev. A* **111**(6), 062404 (2025) <https://doi.org/10.1103/PhysRevA.111.062404>
- [25] Balanis, C.A.: *Advanced Engineering Electromagnetics* (second Edition). John Wiley and Sons, Hoboken, New Jersey (2012)
- [26] Feng, X., Wu, H.: Discontinuous galerkin methods for the helmholtz equation with large wave number. *SIAM J. Numer. Anal.* **47**(4), 2872–2896 (2009) <https://doi.org/10.1137/080737538>
- [27] Shizgal, B.: *Spectral Methods in Chemistry and Physics: Applications to Kinetic Theory and Quantum Mechanics*. Springer, New York (2015)
- [28] Criado, J.C., Spannowsky, M.: Qade: solving differential equations on quantum annealers. *Quantum Sci. Technol.* **8**(1), 015021 (2022) <https://doi.org/10.1088/2058-9565/aca51>

- [29] Borle, A., Lomonaco, S.J.: Analyzing the quantum annealing approach for solving linear least squares problems. In: WALCOM: Algorithms and Computation: 13th International Conference, WALCOM 2019, Guwahati, India, February 27–March 2, 2019, Proceedings 13, pp. 289–301 (2019). https://doi.org/10.1007/978-3-030-10564-8_23 . Springer
- [30] Zbinden, S., Bärtschi, A., Djidjev, H., Eidenbenz, S.: Embedding algorithms for quantum annealers with chimera and pegasus connection topologies. In: High Performance Computing. ISC High Performance 2020. Lecture Notes in Computer Science, vol. 12151, pp. 139–158 (2020). https://doi.org/10.1007/978-3-030-50743-5_10 . Springer
- [31] García-Molina, P., Rodríguez-Mediavilla, J., García-Ripoll, J.J.: Quantum fourier analysis for multivariate functions and applications to a class of schrödinger-type partial differential equations. *Phys. Rev. A* **105**, 012433 (2022) <https://doi.org/10.1103/PhysRevA.105.012433>
- [32] Ng, C.S., Rosenberg, D., Germaschewski, K., Pouquet, A., Bhattacharjee, A.: A comparison of spectral element and finite difference methods using statically refined nonconforming grids for the mhd island coalescence instability problem. *Astrophys. J. Suppl. Ser.* **177**(2), 613 (2008) <https://doi.org/10.1086/588139>
- [33] Asztalos, K., Steijl, R., Maulik, R.: Reduced-order modeling on a near-term quantum computer. *J. Comput. Phys.* **510**, 113070 (2024) <https://doi.org/10.1016/j.jcp.2024.113070>
- [34] Kalinin, K.P., Berloff, N.G.: Computational complexity continuum within ising formulation of np problems. *Commun.Phys.* **20**(5) (2022) <https://doi.org/10.1038/s42005-021-00792-0>
- [35] Wilde, A.C.: Differential equations involving circulant matrices. *Rocky Mountain J. Math.* **13**(1), 1–13 (1983) <https://doi.org/10.1216/RMJ-1983-13-1-1>
- [36] Gilmour, A.E.: Circulant matrix methods for the numerical solution of partial differential equations by fft convolutions. *Appl. Math. Model.* **12**(1), 44–50 (1988) [https://doi.org/10.1016/0307-904X\(88\)90022-4](https://doi.org/10.1016/0307-904X(88)90022-4)
- [37] Davenport, M.A., Laska, J.N., Treichler, J.R., Baraniuk, R.G.: The pros and cons of compressive sensing for wideband signal acquisition: Noise folding versus dynamic range. *IEEE Trans. Signal Process.* **60**(9), 4628–4642 (2012) <https://doi.org/10.1109/TSP.2012.2201149>